Simulation of Explosion by a Coupled FE/DE Gas-Solid Interaction Model

S. Mohammadi[1] **and A. Bebamzadeh**
School of Civil Engineering, University of Tehran, Tehran, IRAN.
[1]Email: smoham@ut.ac.ir

Abstract: *Explosion has always been regarded as one of the most complicated engineering problems. As a result, many engineers have preferred rather simplified empirical approaches in comparison to extremely complex deterministic analyses. In this paper, however, a numerical simulation based on the combined finite/discrete element methodology is presented for analyzing the dynamic behavior of fracturing rock masses in blasting. A finite element discretization of discrete elements allows for complex shapes of fully deformable discrete elements with geometric and material nonlinearities to be considered. Only a Rankine strain softening plasticity model is employed, which is suitable for rock and other brittle materials. Creation of new lines/edges/bodies from fracturing and fragmentation of original objects is systematically considered in the proposed gas-solid interaction flow model. An equation of state is adopted to inexpensively calculate the pressure of the detonation gas in closed form. The model employed for the flow of detonation gas has resulted in a logical algorithmic procedure for the evaluation of spatial distribution of the pressure of detonation gas, work done by the expanding gas and the total mass of the detonation gas as functions of time; indicating the ability of model to respond to changes in both the mass of explosive charge and the size of the solid block undergoing fracture. Rock blasting and demolition problems are amongst the engineering applications that are expected to benefit directly from the present development. The results of this study may also be used to provide some numerical based reliable solutions for the complex analysis of structures subjected to explosive loadings.*

Keywords: *Explosion, rock blasting, gas solid interaction, combined finite/discrete element method.*

1. Introduction

Majority of analytical and numerical methods of investigating the strength of materials are based on the continuum mechanics and the classical theory of plasticity which maintain the continuity of the domain while performing nonlinear failure controls. Nevertheless, many engineering/industrial applications such as blasting in mines, demolition of structures, crushing, metal cutting etc. are primarily designed based on the cracking and fracturing potential of materials. In these classes of problems, controlled failure and cracking of material are as desirable as the strength of material.

From an industrial prospective, explosion is one of the cheapest operational techniques for fragmentation of solid material, though less delicate and accurate than other available methods. For instance, by detonating the explosive material filled in existing boreholes, large rock masses are cracked and fragmented into small pieces. Unfortunately, there exist only some general controls on the size limits of fragments.

On the other hand, from a computational prospective, numerical modeling of an intact or fractured medium subjected to explosive loading is one of the most difficult applications involving various mechanical behaviors in various fields such as plasticity, fracture mechanics, gas dynamics and chemical/mechanical behavior of detonation and explosion phenomena. In addition, a strong coupling is expected between the gas and solid phases. Detonation causes a phase

change of the explosive material into a gas with high pressure and temperature. The amount of release of energy depends on the specific energy (energy per unit mass) of the solid explosive material. Part of this energy is transmitted to the solid mass and causes subsequent deformation, acceleration, fracture and fragmentation of the solid material. Gas expansion and its flow within the crack openings as well as the energy consumption for solid deformation reduce the gas pressure. Therefore, gas explosion and cracking are strongly coupled phenomena; applying the gas pressure onto the solid body while changing gas characteristics by deformation and cracking of the solid material.

A wide range of blast induced gas pressure models have been proposed [1-8]. The earliest model, dating back to 1899, is the Rankine-Hugoniot model for blast shock waves based on the mass, momentum and energy conservation equations [1-2]. A century later, they are still the backbone of blast and shock wave simulations. The simplest model, however, is a user defined pressure-time curve which lacks any interaction phenomena [3-4]. As a result, such an analysis becomes sensitive to the way user defines the pressure curve. On the other hand, several gas flow models have been developed which somehow simulate the gas flow within the crack opening [5-14]. They are mainly based on two approaches; detecting the gas flow within independent cracks, and detecting an equivalent flow within a porous medium simulated from the cracked solid mass. The first approach involves with rather difficult contact detection algorithms for detecting the gas flow within the complex geometry of independent cracks, while the second approach requires a realistic estimation of porosity [11-14].

A comprehensive approach which adopts two separate but coupled meshes for the analysis of solid and gas phases is proposed for the study of the gas-solid interaction and simulation of explosion. In gas phase, equations of gas flow in a porous medium are used to compute the pressure, mass transfer, energy and expansion of the gas at each specified point. The solution for the solid state will be performed based on the derived pressure loading.

Modelling the solid media is performed by the combined finite/discrete element methodology [14-17]. It is capable of analyzing the interaction among a wide range of discrete bodies/materials and is coupled, in this study, with gas dynamics and porous media equations to analyze the dynamic behavior of fracturing media in blasting. A Rankine strain softening plasticity model, which has been widely used for simulation of cracking in brittle materials, is employed for modeling creation and propagation of cracks [18].

When the gas-solid interaction model is implemented into the combined finite/discrete element method, the model will be capable of the evaluation of spatial distribution of the pressure of detonation gas, work done by the expanding gas and the total mass of detonation gas as functions of time indicating the ability of the model to respond to changes in both the mass of explosive charge and the size of the fractured solid block. The proposed algorithm allows for corporation of gas flow interaction with new changing geometry of fractured solid model.

2. Porous Media

Microscopic and macroscopic equations of state have already been developed to study

Fig.1 Flow through a typical porous specimen.

different physical behaviour of gas and solid phases of a porous medium [18]. Each phase may be considered separately or studied within a multi-phase porous medium. Here, only the necessary two dimensional equations of conservation of mass and momentum are examined. Figure 1 illustrates typical 2D porous specimens with the emphasis being on the potential fluid/gas flow within the networks of interstitial spaces [17].

The differential form of the balance equation for variable $\overline{\psi}^{\pi}$, a macroscopic thermodynamic property associated with a π–phase, can be derived under certain smoothness conditions by localization at the macroscopic level [18]

$$\frac{\partial}{\partial t}(<\rho>_{\pi}\overline{\psi}^{\pi}) + div(<\rho>_{\pi}\overline{\psi}^{\pi}\overline{\mathbf{V}}^{\pi}) - div\mathbf{i}^{\pi} - <\rho>_{\pi}[\overline{b}^{\pi} + e^{\pi}(\rho\psi) + I^{\pi}] =<\rho>_{\pi}\overline{G}^{\pi} \quad (1)$$

subject to

$$\sum_{\pi}(\rho)_{\pi}[e^{\pi}(\rho\psi) + I^{\pi}] = 0 \quad (2)$$

where the exchange of $\overline{\psi}^{\pi}$ due to mechanical interactions between the constituents is given by

$$I^{\pi} = \frac{1}{<\rho>_{\pi} dV}\sum_{\alpha\neq\pi}\int_{da^{\pi\alpha}}\mathbf{n}^{\pi\alpha}.\mathbf{i}\ da_m \quad (3)$$

and the phase change of a constituent or possible mass exchange between the constituent π and the other constituents α is given by

$$e^{\pi}(\rho\psi) = \frac{1}{<\rho>_{\pi} dV}\sum_{\alpha\neq\pi}\int_{da^{\pi\alpha}}\rho\psi(\mathbf{W}-\dot{\mathbf{r}}).\mathbf{n}^{\pi\alpha}da_m \quad (4)$$

where other parameters are defined as

$\mathbf{i}^{\pi}$ = the flux vector associated with $\overline{\psi}^{\pi}$
$\overline{b}^{\pi}$ = the external supply of $\overline{\psi}^{\pi}$
$\overline{G}^{\pi}$ = the net production of $\overline{\psi}^{\pi}$
$<\rho>_{\pi}$= the volume-averaged value of mass density
r = the position of a microscopic volume element
$\dot{r}$ = the velocity of the phase at a fixed point in space
$n^{\pi\alpha}$ = the unit normal vector pointing out of the π phase and into the α phase

If the body is separated by a discontinuity surface G which moves with velocity $\overline{w}$ at the macroscopic scale, the following additional relation must be fulfilled:

$$[<\rho>\overline{\psi}_{\pi}^{\pi}(\overline{\mathbf{V}}^{\pi} - \overline{\mathbf{W}}) - \mathbf{i}^{\pi}].\mathbf{N} = 0 \quad (5)$$

Different equations can be derived by properly defining ψ, i,b and G variables.

The mass balance equation for solid and/or gas phases based on a microscopic viewpoint can be defined as:

$$\frac{\partial\rho}{\partial t} + div(\rho\dot{\mathbf{r}}) = 0 \quad (6)$$

while on a macroscopic level, the mass

balance equation for the solid phase (s) can be written as:

$$\frac{D^s(1-n)\rho^s}{Dt} + \rho^s(1-n)div\overline{\mathbf{V}}^s = 0 \qquad (7)$$

where $\rho^s = <\rho>^s_s$ is the intrinsic phase averaged density, stands for the phase averaged solid density and is the mass averaged solid velocity.

Similarly, for the gas phase,

$$\frac{\partial}{\partial t}(n\rho^g) + div(n\rho^g \mathbf{V}^g) = 0 \qquad (8)$$

Equation for the microscopic linear momentum balance takes the following form

$$div\ \mathbf{t}_m + \rho(\mathbf{g} - \ddot{\mathbf{r}}) = 0 \qquad (9)$$

where t_m is the microscopic stress tensor and g is the external momentum supply related to gravitational effects. The macroscopic linear momentum, however, takes a more complicated form,

$$\eta^\pi \mathbf{V}^{\pi s} = \frac{\mathbf{k}k^{r\pi}}{\mu^\pi}[-\nabla p^\pi + \rho^\pi(\mathbf{g} - a^s - a^{\pi s})] \qquad (10)$$

where η^π is the volume fraction, μ^π is the dynamic viscosity, $a^{\pi s}$ is the relative acceleration, k is the permeability tensor of the medium, and $k^{r\pi}$ is the relative permeability parameter.

Equation (10) reduces to the well known Darcy law by neglecting the relative and solid phase accelerations in comparison to very high pressures,

$$\eta^\pi \mathbf{V}^{\pi s} = \frac{\mathbf{k}k^{r\pi}}{\mu^\pi}[-\nabla p^\pi + \rho^\pi \mathbf{g}] \qquad (11)$$

and if further neglecting the gravitational acceleration g and $V_s = 0$,

$$n\mathbf{V}^g = \frac{\mathbf{k}k^{rg}}{\mu^g}(-\nabla p^g) \qquad (12)$$

Combining the mass and momentum equations leads to

$$\frac{\partial}{\partial t}(n\rho^g) + div\left[\frac{\mathbf{k}k^{rg}\rho^g}{\mu^g}(-\nabla p^g)\right] = 0 \qquad (13)$$

Finally, microscopic and macroscopic energy balance equations can be written as:

$$\frac{\partial}{\partial t}(\rho E + \rho\frac{1}{2}\dot{\mathbf{r}}.\dot{\mathbf{r}}) + div[\rho(E + \frac{1}{2}\dot{\mathbf{r}}.\dot{\mathbf{r}})\dot{\mathbf{r}}] \qquad (14)$$

$$\sum_\pi \rho_\pi[\mathbf{e}^\pi(\rho\hat{E}) + \mathbf{e}^\pi(\rho\dot{\mathbf{r}}).\overline{\mathbf{V}}^\pi + \frac{1}{2}e^\pi(\rho)\overline{\mathbf{V}}^\pi.\overline{\mathbf{V}}^\pi + \hat{\mathbf{t}}^\pi.\overline{\mathbf{V}}^\pi + Q^\pi] = 0 \qquad (15)$$

where E is the specific intrinsic energy, is the heat flux vector, h is the intrinsic heat source and Q^π is the exchange of energy due to mechanical interaction.

3. Coupled Gas-Solid Interaction

In this section, an interaction algorithm based on a two-mesh model is developed. One mesh is used for modeling the solid material (S-mesh) and the second mesh is used for modeling the gas phase (G-mesh), as illustrated in Figure 2. At any time t, the G-mesh can be mapped onto the S-mesh, and all necessary data can be transferred from the S-mesh to the G-mesh for evaluation of the gas porosity [19].

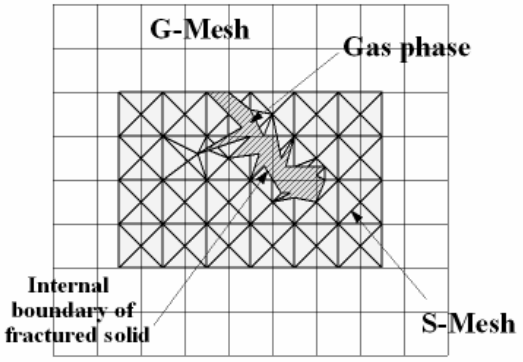

Fig.2 Coupled s-mesh and g-mesh finite element model.

The G-mesh is analyzed based on the mechanics of porous media; it is assumed that no solid exists for the gas phase and only the equations of mass and momentum are satisfied. The solid phase contributes the equilibrium equation only through the permeability coefficient, defined for example,

$$\mathbf{k} = \mathbf{k}_{\max}\left(\frac{dv_g}{dv}\right) \tag{16}$$

$$dv_g = dv - dv_s \tag{17}$$

Beginning with the mass-momentum equation for the gas phase,

$$\frac{\partial}{\partial t}(\rho^g) + div\left[\frac{\mathbf{k}k^{rg}\rho^g}{\mu^g}(-\nabla p^g)\right] = 0 \tag{18}$$

with the boundary conditions

$$\rho^g \frac{\mathbf{k}k^{rg}}{\mu^g}(-\nabla dp^g)^T.\mathbf{n} = q^g \ \ on \qquad \Gamma_g^q \tag{19}$$

where q^g is the input mass flow and $n=\{n_x, n_y, n_z\}^T$ is the normal vector.

The weighted residual form of (18) and (19) can be written as [19]

$$\int_\Omega \mathbf{W}^{*T}\left\{\nabla^T\left[\frac{\mathbf{k}}{\mu^g}(-\nabla p^g)\right] + \frac{\partial \rho^g}{\partial t}\right\}d\Omega + \int_{\Gamma_g^q}\overline{\mathbf{W}}^{*T}\left[\frac{\mathbf{k}}{\mu^g}(-\nabla p^g)^T.\mathbf{n} - \frac{q^g}{\rho^g}\right]d\Gamma = 0 \tag{20}$$

where $\overline{\mathrm{W}}^*$, W^* are weighted residual functions. Applying the Green theorem

$$\int_\Omega\left[(\nabla \mathbf{W}^*)^T\frac{\mathbf{k}\rho^g}{\mu^g}\nabla p^g) + \mathbf{W}^{*T}\frac{\partial \rho^g}{\partial t}\right]d\Omega + \int_{\Gamma_g^q}\mathbf{W}^{*T}\frac{q^g}{\rho^g}d\Gamma = 0 \tag{21}$$

and assuming $q^g = 0$,

$$\int_\Omega(\nabla \mathbf{W}^*)^T\frac{\mathbf{k}\rho^g}{\mu^g}\nabla p^g d\Omega + \int_\Omega \mathbf{W}^{*T}\frac{\partial \rho^g}{\partial t}d\Omega = 0 \tag{22}$$

Following the standard finite element procedure, pressure P^g can be defined based on the nodal pressure $\overline{P}^g$ and the nodal shape function N_p,

$$P^g = \mathbf{N}_p\overline{P}^g \tag{23}$$

The weighted residual functions are assumed to be the same as shape functions

$$\mathbf{N}_p = \mathbf{W}^* \tag{24}$$

Therefore, equation (22) reduces to

$$\int_{d\Omega}(\nabla \mathbf{N}_p)^T\frac{\mathbf{k}\rho^g}{\mu^g}\nabla \mathbf{N}_p\overline{\mathbf{P}}^g d\Omega + \frac{1}{\partial t}\int_\Omega \mathbf{N}_p^T\partial\rho^g d\Omega = 0 \tag{25}$$

The first term represents the change of mass in unit time. The final form can be written as [19]

$$\mathbf{M}_{t+\Delta t} = \mathbf{M}_t - \Delta t\mathbf{H}_t^p\overline{\mathbf{P}}_t^g \tag{26}$$

with H_t^p defined as the permeability matrix,

$$\mathbf{H}_t^p = \int_\Omega(\nabla \mathbf{N}_p)^T\frac{\mathbf{K}\rho^g}{\mu g}\nabla \mathbf{N}_p d\Omega \tag{27}$$

By adopting a square cell G-mesh (Figure 3), shape functions can be written as:

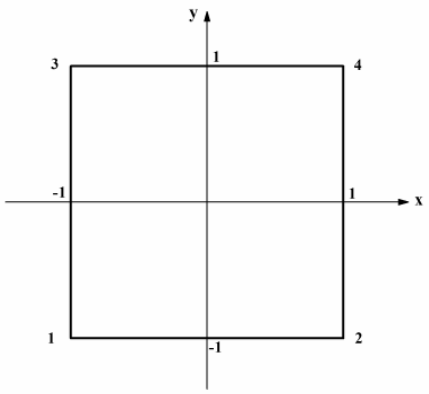

Fig.3 Square element for the G-mesh

$$\mathbf{N}_p = 0.25[(1-x)(1-y),(1+x)(1-y),(1-x)(1+y),(1+x)(1+y)] \quad (28)$$

and

$$d\Omega = a^2 dxdy \quad (29)$$

where a is the size of the square element.
If the mean values of $\bar{\rho}_g$ and $\bar{K}$ are used over the element and assuming μ_g = 1, a simple H_t^p matrix can be computed [19]

$$\mathbf{H}_t^p = \frac{1}{6} a^2 \bar{\rho}_g \bar{K} \begin{bmatrix} 4 & -1 & -1 & -2 \\ -1 & 4 & -2 & -1 \\ -1 & -2 & 4 & -1 \\ -2 & -1 & -1 & 4 \end{bmatrix} \quad (30)$$

However, a more accurate solution is achieved if similar shape functions are used to approximate the variations of density and porosity within the element. Numerical solutions are then required to evaluate the components of symmetric H_t^p matrix.

Returning to the mass equation (26) for an element e,

$$\mathbf{M}_{t+\Delta t}^e = \mathbf{M}_t^e - \Delta t \mathbf{H}_t^p \mathbf{P}_t \quad (31)$$

Similar equation can be derived for the change of internal energy, in terms of the mean internal energy per unit mass of the element $\bar{U}_e$

$$\mathbf{U}_{t+\Delta t}^e = \mathbf{U}_t^e - \Delta t \bar{U}_e \mathbf{H}_t^p \mathbf{P}_t \quad (32)$$

A non-perfect gas law is adopted to include for the high pressure and temperature conditions (where the gas can not be considered as a perfect gas),

$$P = \bar{R} \frac{\rho}{1 - \rho e^{-0.4\rho}} T \quad (33)$$

Another necessary assumption is the way $V_s(p)$; the volume of a solid at mean pressure p, can be calculated from its volume at zero pressure state V_s(o),

$$V_s(p) = V_s(\mathrm{o}) * e^{-p/\lambda} \quad (34)$$

where λ is the rate of volume reduction.

The step by step procedure for the developed gas flow algorithm can be explained as:

1. Set the initial values for the G-mesh nodes M_n^o , p_n^o , U_n^o.

2. Evaluate the solid volume associated to each node of the G-mesh.

3. Calculate the solid volume at pressure p, $V_{s,n}^o = V_{s,n}^o(0) e^{-p/\lambda}$

4. Calculate the porosity volume of the G-mesh nodes $V_{p,n}^o = V_n^o - V_{s,n}^o$, V_n^o is the volume of G-mesh nodes without any solid

5. Compute the initial mean density ($\bar{\rho}$) from $\rho_n^o = M_n^o / V_{p,n}^o$ and the initial permeability of the element $K_o = K_{max}(V_p^o / V^o)$

6. Calculate the permeability matrix H_{pe}^o

7. Calculate the mean internal energy per unit mass $\bar{U}_e^o$ from its nodal values U_n^o

8. Determine new nodal pressures

9. Interpolate the S-mesh nodal pressures from the G-mesh nodal values

10. Analyze the solid model using an explicit dynamic FE/DE analysis

11. Perform a deformation/crack analysis based on the material model for the solid, and perform re-meshing and geometric crack modeling, if necessary

12. Compute the deformation and new values

for porosity in G-mesh

13. The new value for the mass is computed from the nodal pressures P_n , $M_n^1 = M_n^o - \Delta t\, H_{pe}^o P_n^o$

14. The new value for the internal energy $U_n^1 = U_n^o - \Delta t\, \bar{U}_e^o H_{pe}^o P_n^o$ has to be corrected due to the change of G-mesh nodal volumes and porosities

Step 8 requires a simple iterative procedure for determining new pressure values which is now briefly explained:

1. Set the initial values for $i=0$

$P_n^1 = P_n^{1,o} = P_n^o$

$V_{s,n}^{l,i} = V_{s,n}^1 (P_n^{1,i})$

$V_{p,n}^{1,o} = V_n^1 - V_{s,n}^{l,i}$

2. Calculate the work done by the gas due to change of porosity

$\Delta W^i = P_n^o (V_{p,n}^{1,o} - V_{p,n}^o)$

$U_n^{i,l} = U_n^1 - \Delta W^i$

$T_n^{i,l} = U_n^{i,l} / (C_V M_n^1)$

3. Calculate the new pressure from the gas pressure law

$P_n^{l,i} = P (\rho_n^{l,i}, T_n^{l,i})$

4. If $\left| P_n^{l,i} - P_n^{l,i-1} \right| \geqq \in$, Set $i=i+1$ and goto 2

The final remaining important point is the selection of a proper timestep size, as it directly affects the accuracy, cost and efficiency of the numerical simulation. In a practical simulation, size of the timestep has to be selected from the characteristics of both phases:

1. Δt for the solid phase:
An explosion in a solid is accompanied by very high pressure, extensive cracking and fragmentation. Therefore, the timestep Δt must be limited to a value necessary to perform contact detection and interaction procedures to avoid cracked elements or discrete elements to excessively penetrate or fly through each other freely [17].

2. Δt for the gas phase:
Δt is one of the effective terms in defining the mass update according to $M_{t+\Delta t} = M_t - \Delta t\, H_p^t P_g$. Δt should then be fine tuned so the gas flow is performed at the same time as the cracks are opened. Too small timestep results in small mass transfer into cracks; no gas flow within opening cracks. On the other hand, too large timesteps cause large mass transfers to occur without any crack opening.

4. Solid Fracture

Cracking and Fragmentation in solid domain is performed based on a softening plasticity formulation. As a result, fracture mechanics concepts such as toughness, etc. are not required. Here, a simple bilinear Rankine softening law (Figure 4) is adopted to avoid mesh dependency of the finite element

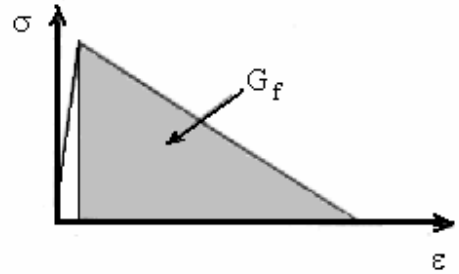

Fig.4 Strain softening model and the definition of fracture energy release G_f.

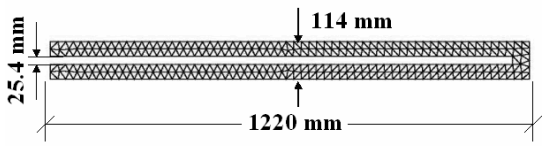

Fig.5 Triangular finite element mesh for modeling the solid chamber.

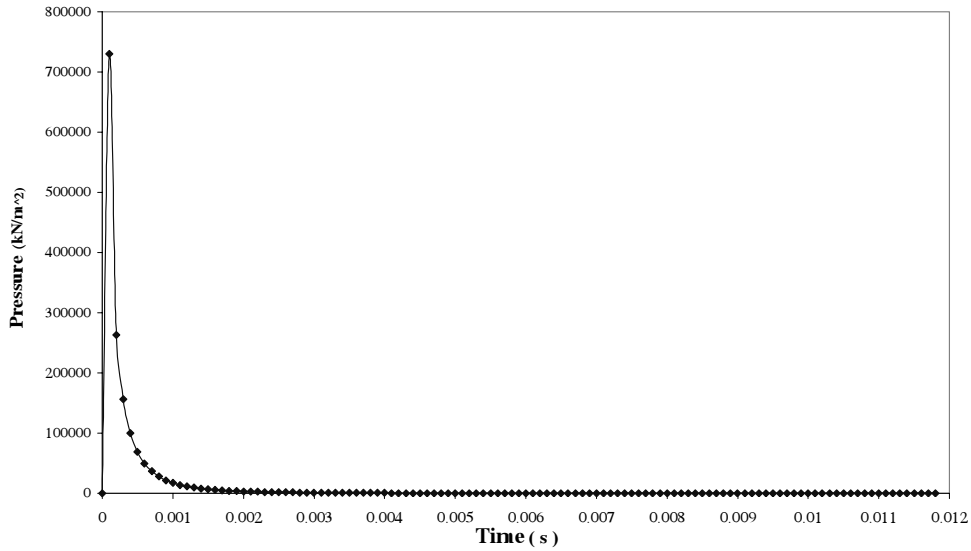

Fig.6 Pressure history response predicted by the present algorithm.

simulation through the introduction of the fracture energy release G_f and a charachteristic length. Special remeshing techniques are adopted in order to geometrically simulate the crack propagation by splitting the necessary finite elements and nodes and satisfaction of compatibility requirements [18]. Therefore, the new finite/discrete element mesh conforms to the cracked and fragmented geometry of the solid domain, and can be directly used through the gas flow procedure.

5. Numerical Verification

5.1 Example 1

This example is adopted to verify the gas flow algorithm in its simplest possible case: gas flow through a uniform pipe. A solid chamber is filled with ANFO explosive material, as illustrated in Figure 5. The density of explosive material is $\rho = 240\, kg/m^3$and the total mass is $m = 0.148\, kg$. The velocity of detonation (VOD) is assumed to be $1725 m/s$.

The gas pressure history, predicted by the proposed approach is illustrated in Figure 6. It almost instantly reaches to a peak value of 730000 KN/m^2 and then gradually reduces to atmospheric pressure (zero overpressure). The results are in very good agreement with the experimental measurements and the results obtained by Munjiza [4] based on a single mesh gas dynamics (no flow)

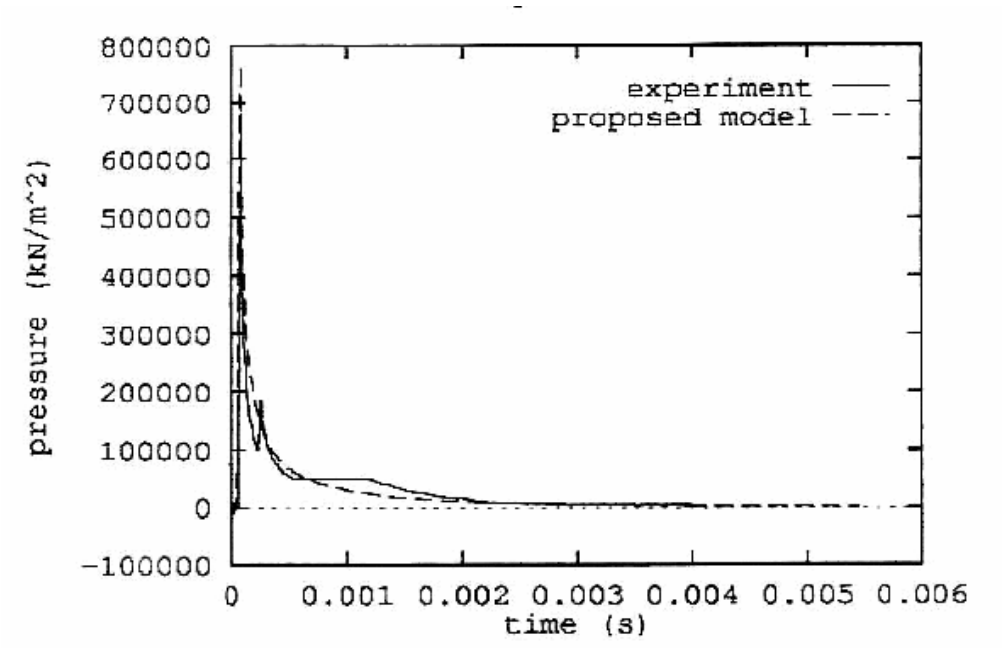

Fig.7 Pressure history response reported by Munjiza [4].

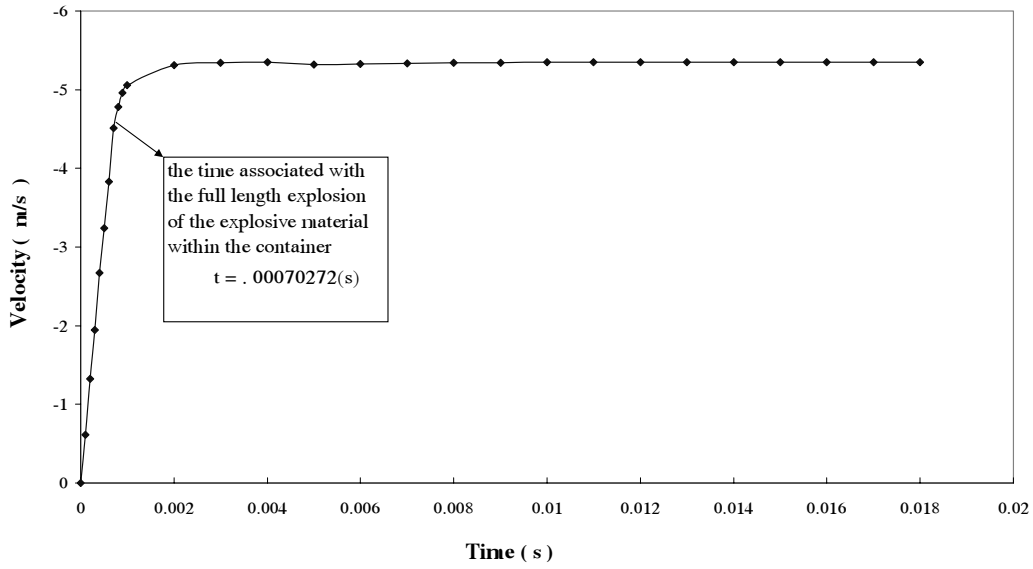

Fig.8 Velocity history of the solid chamber.

approach (Figure 7).

Figure 8 illustrates the velocity time history of the chamber. It shows the point of completion of explosion process within the chamber, where a sudden change of slope is predictable.

Deformation and effective stress contours at successive timesteps are illustrated in Figures 9-10. Again, as the detonation of the explosive material extends towards the free

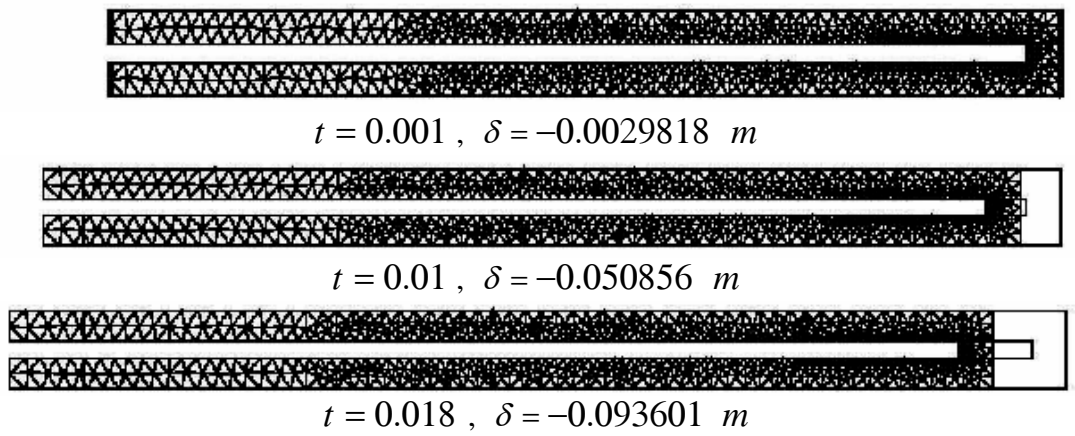

Fig.9 Displacement of the container at successive timesteps.

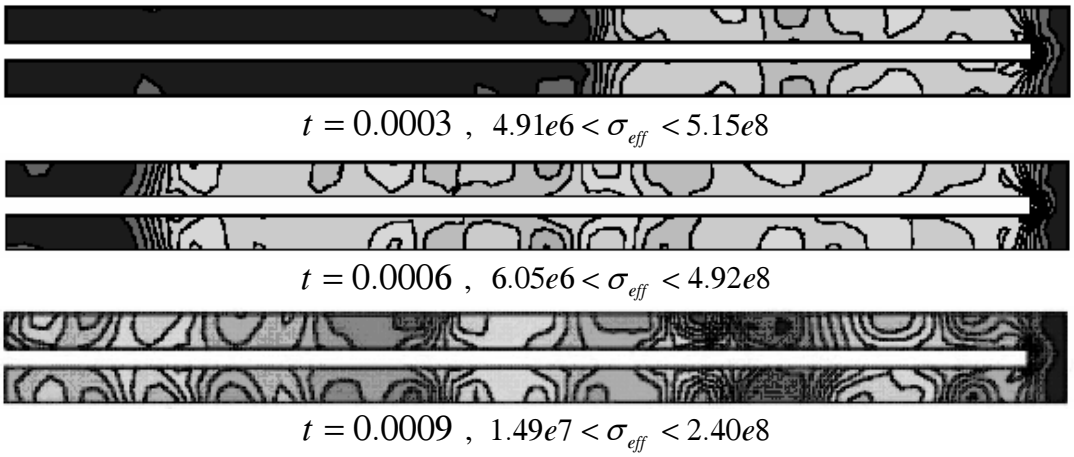

Fig.10 Effective stress contours on the container at successive timesteps.

end of the container, the stress bubbles continuously move from the right end of the container towards its free end.

5.2 Example 2

This is a complex example of gas-solid interaction problem modelled by a two-mesh approach within a finite/discrete element approach. Consider a $1\times1\,m$ square block of rock with $0.33\times0.33\,m$ a central hole (Figure 11a). The hole is completely filled with ANFO explosive material. Properties of rock and explosive materials are given in Table 1.

Table 1 Material properties.

Rock	ANFO Explosive
$E = 28000\ (MPa)$	$\rho = 850\ (kg/m^3)$
$v = 0.1$	$VOD = 1725\ (m/s)$
$\rho = 4200\ (kg/m^3)$	$Q_e = 3700\ (kJ/kg)$
$G_f = 250(N.m/m^2)$	$\lambda = 1.2\times10^{10}$
	$\mathbf{K} = 3\times10^{-8}\ (m^2/pa.s)$
	$t_G = 1e^{-9}$

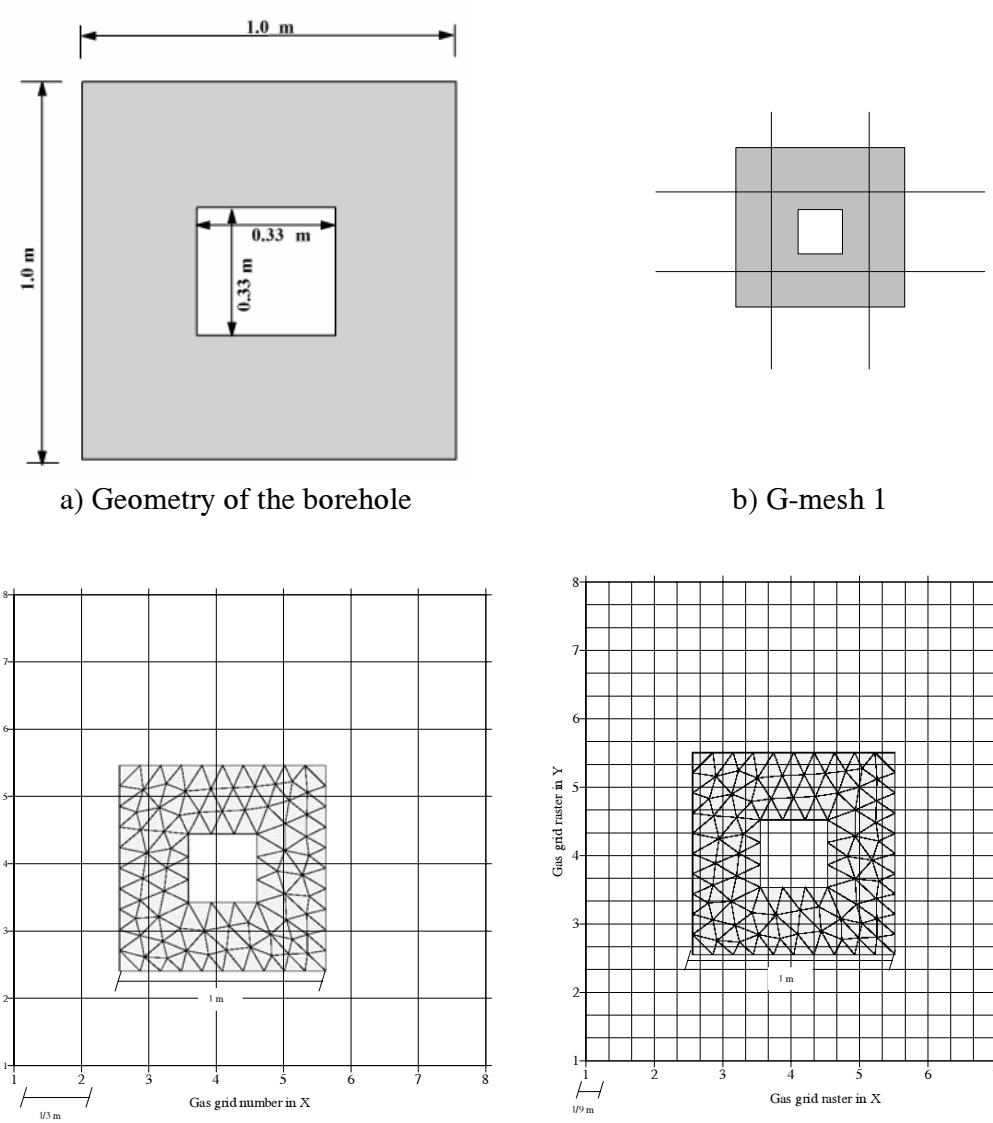

a) Geometry of the borehole

b) G-mesh 1

c) G-mesh 2 and the solid mesh

d) G-mesh 3 and the solid mesh

Fig.11 Geometry and different gas and solid meshes.

Three different meshes (depicted in Figure 11b,c,d) have been used to investigate the effect of gas mesh density.

Mesh 1 is a very coarse mesh which does not have any point inside the explosion hole (borehole). As a result, no gas pressure can be evaluated at the gas-mesh nodes. Therefore, no pressure on solid mesh is generated.

The second G-mesh, mesh 2, is defined in a region two times the dimensions of the solid rock. 8 square elements are used in each direction. It is expected to achieve poor results again, because of having only one node of the gas mesh (node (4,4)) within the explosion borehole

The third mesh is constructed using 24 square elements in each direction. Nine gas

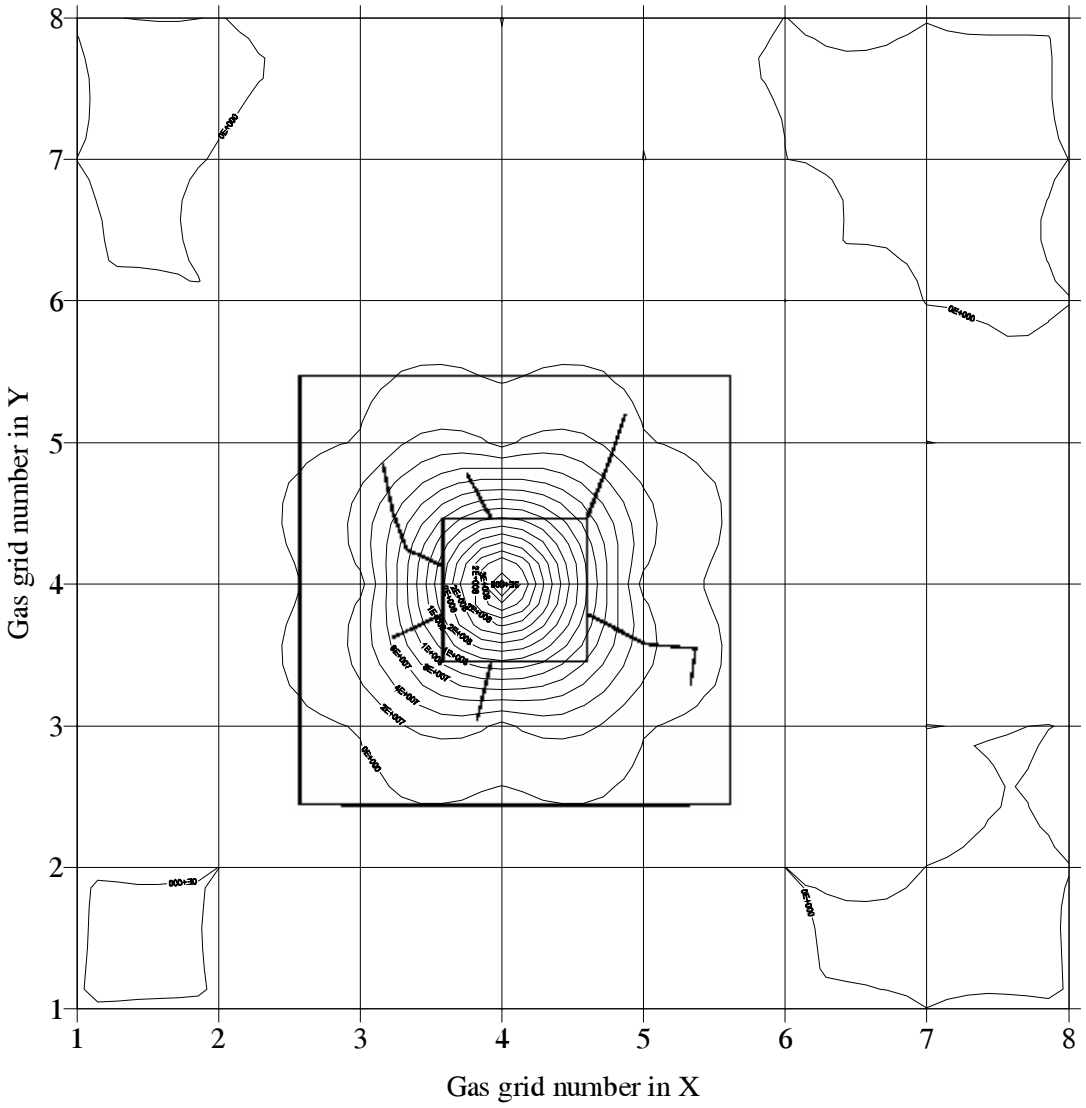

Fig.12 Cracking pattern and gas pressure contour at t=0.0003

nodes are located within the explosion borehole. Better approximation may be achieved by adopting finer gas mesh. It is important to note that there should be a practical limit on the minimum size of the gas mesh as the cost of numerical simulation may be unacceptably increased with a very small size of the gas mesh.

Figures 12-14 illustrate the pressure contours and cracking patterns in different timesteps. By increasing the openings of cracks, part of the gas mass is transferred through the openings; instantly increasing the gas pressure in the vicinity of cracks. This is clearly seen from Figure 13 where the values of gas pressure are greater in the top left part of the solid mesh with extensive cracking. The pressure substantially reduces immediately after the escape of gas from the crack opening.

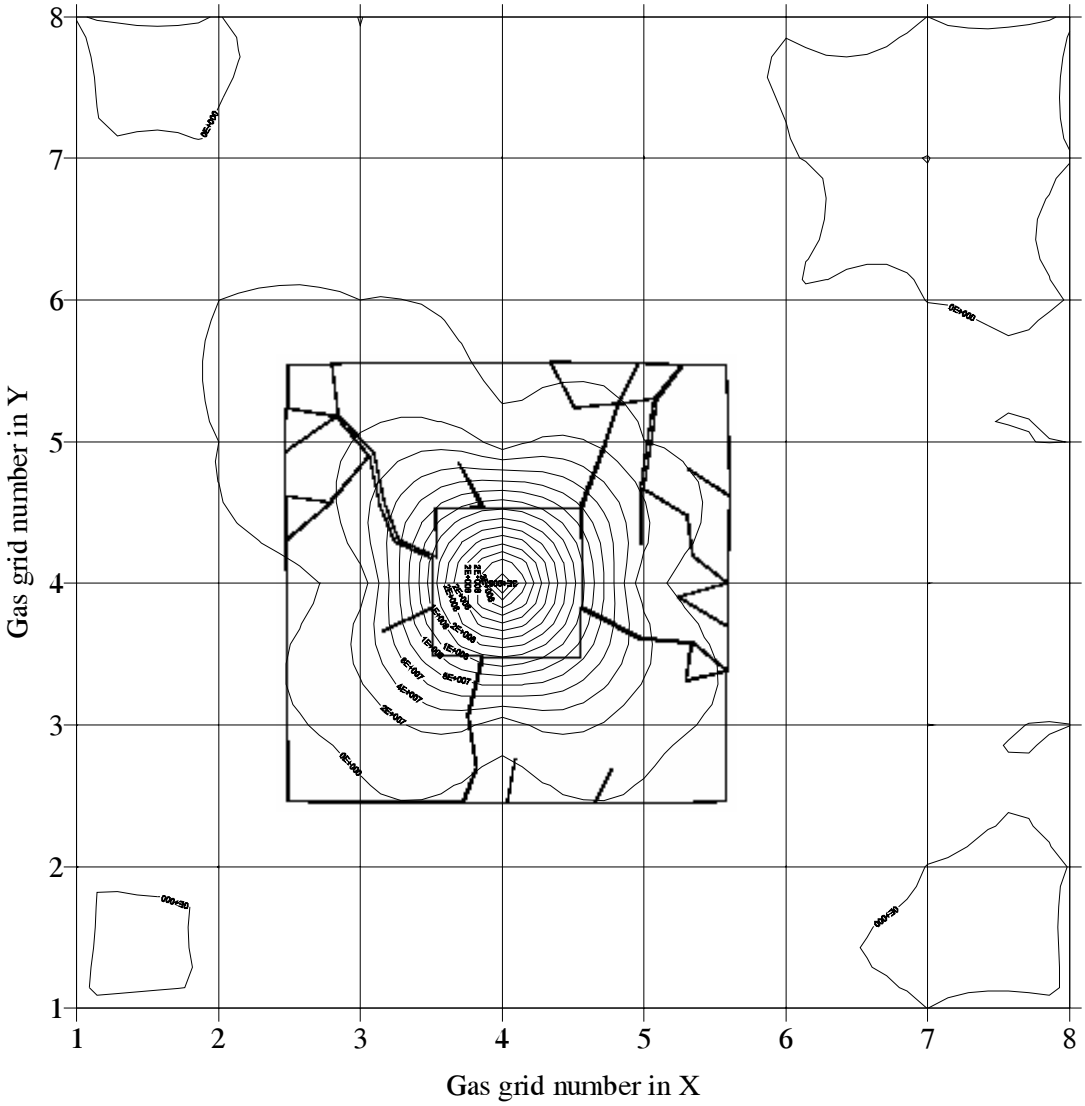

Fig.13 Cracking pattern and gas pressure contour at t=0.0006

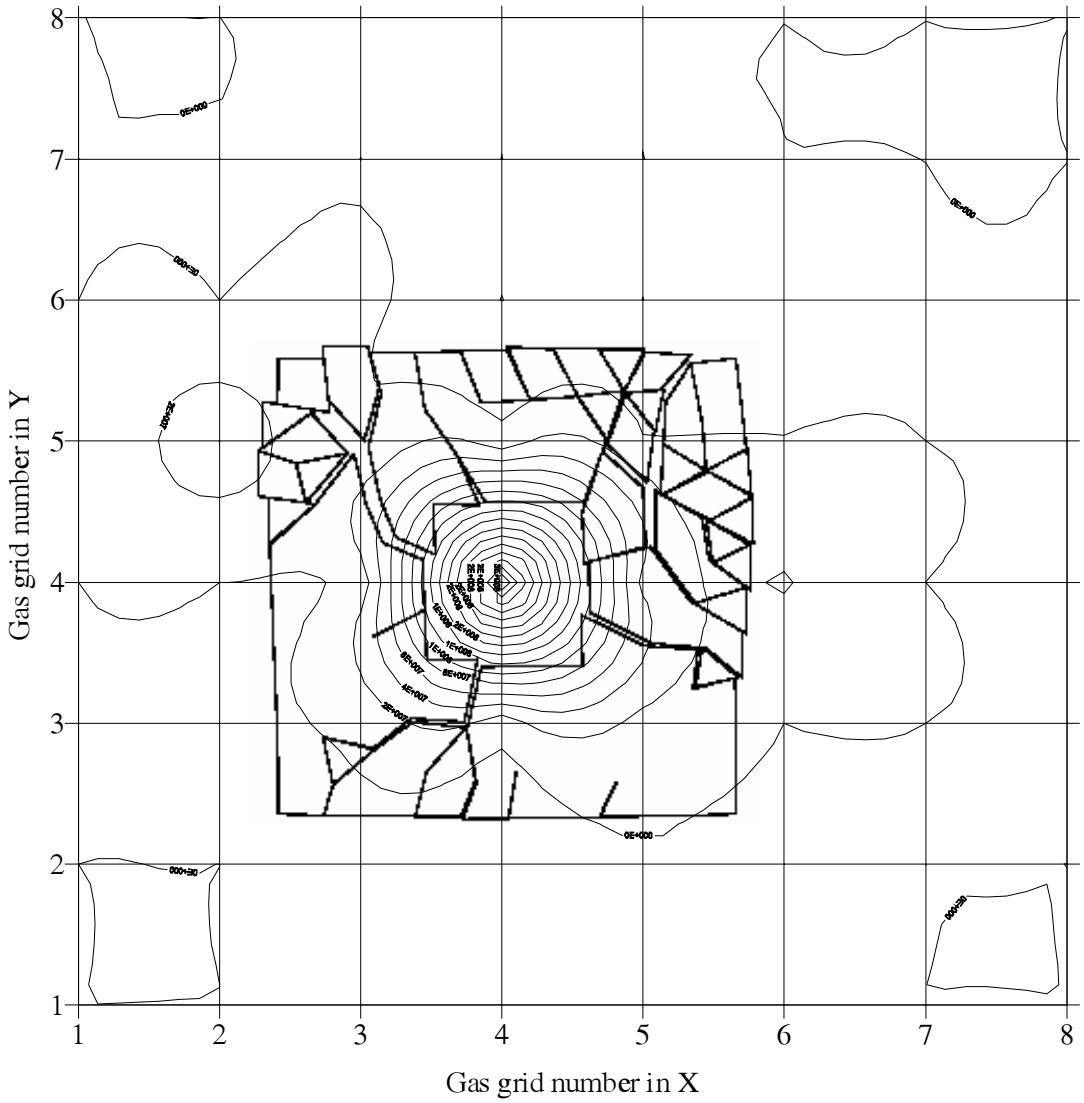

Fig.14 Cracking pattern and gas pressure contour at t=0.001

6. Conclusion

A finite element based gas flow within an equivalent porous solid medium has been developed for the analysis of gas-solid interaction and implemented into a combined finite/discrete element methodology to simulate the complex behavior of explosion in solid media which causes extensive fracture and fragmentation within the domain; affecting the pressure and density of the gas induced by blast. Numerical simulations have shown good agreement with available benchmarks. The proposed approach solves the equations of gas flow and solid state by adopting a coupled two-mesh strategy. It is proposed to design an independent adaptive gas mesh in future studies.

7. References

[1] Chapman, D.L. (1899); On the rate of explosion in gases. Philosophical Magazine. 213, Series 5 (47), 90.

[2] Joughet, E. (1905); Sur la propagation des reactions chiiques dans la gaze. Journal of Pure and Applied Mathematics 70, Series 6 (1), 347.

[3] Johnsson, C.H. and Persson, P.A. (1970); Detonics of high explosives. Academic Press: London, UK.

[4] Bauer, A.A. and Fratzos, D. (1987); Finite element modeling of pre-split blasting using measured time curves. Society of Explosive Engineers Annual Meeting, Miami, USA.

[5] Xian, L. and Bicanic, N. and Owen, D.R.J. and Munjiza A. (1991); Rock blasting simulation by rigid body dynamic analysis and rigid brittle fracturing model. Proceedings of the international conference on nonlinear engineering computations, NEC-91, Pineridge Press, Swansea, UK; pages: 477-587.

[6] Preece, D.S. and Burchell, S.L. and Scovira, D.S. (1993); Coupled gas flow and rock motion modeling with comparison to bench blast field data. In Proceedings Fragblast-4; 239-247.

[7] Nilson, R.H. (1996); An integral method for predicting hydraulic fracture propagation driven by gases or liquids. International journal of rock Mechanics; 22:3-19.

[8] Preece, D.S. and Thorne, B.J. (1996); A study of detonation timing and fragmentation using 3D finite element techniques and damage constitutive model. In Proceeding Fragblast-5; 147-156.

[9] Daehnke, A. and Rossmanith, H. and Schatz, J.F. (1997); On dynamic gas pressure induced fracturing. International journal of blasting and fragmentation; 1:59-73.

[10] Hustrulid, W. (1999); Blasting principles for open pit mining, Theoretical Foundations, Volume 2, A.A. Balkema, Netherlands.

[11] Danell, R.E. and Lewnardowski, T. and Laun Mai, V.K. (1997); Influence of discontinuities on pre-splitting effectiveness. International journal of blasting and fragmentation; 1:27-41.

[12] Persson, P.A. (1997); The relationship between stain energy, rock damage,

fragmentation and throw in rock blasting. International journal of blasting and fragmentation; 1:73-99.

[13] Minchinton, A. and Lynch, P. (1997); Fragmentation and have modeling using coupled discrete element gas flow code. International journal of blasting and fragmentation; 1:49-59.

[14] Munjiza, A. and Latham J.P. and Andrews, K.F. (2000); Detonation gas model for combined finite-discrete element simulation of fracture and fragmentation". International journal for numerical methods in engineering; 49:1495-1520

[15] Munjiza, A. (1992); Discrete elements in transient dynamics of fractured media. Ph.D. thesis, University of Wales Swansea.

[16] Munjiza, A. and Owen, D.R.J. and Bicanic, N. (1995); A combined finite-discrete element method in transient dynamics of fracturing solids. International journal of engineering computations; 12: 145-174.

[17] Mohammadi, S. (2003); Discontinuum Mechanics Using Finite and Discrete Elements, WIT Press, UK.

[18] Lewis, R.W. and Schrefeler, B.A. (1998); The Finite Element Method in the Static and Dynamic Deformation and Consolidation of Porous Media. Second edition. England.

[19] Bebamzadeh, A. (2004); Simulation of explosion by a combined finite discrete element method. MSc Thesis, University of Tehran.